JOURNAL OF COMPUTATIONAL PHYSICS 48, 387–411 (1982)

High-Re Solutions for Incompressible Flow Using the Navier–Stokes Equations and a Multigrid Method*

U. GHIA, K. N. GHIA, AND C. T. SHIN

University of Cincinnati, Cincinnati, Ohio 45221

Received January 15, 1982

The vorticity–stream function formulation of the two-dimensional incompressible Navier–Stokes equations is used to study the effectiveness of the coupled strongly implicit multigrid (CSI–MG) method in the determination of high-Re fine-mesh flow solutions. The driven flow in a square cavity is used as the model problem. Solutions are obtained for configurations with Reynolds number as high as 10,000 and meshes consisting of as many as 257×257 points. For $Re = 1000$, the (129×129) grid solution required 1.5 minutes of CPU time on the AMDAHL 470 V/6 computer. Because of the appearance of one or more secondary vortices in the flow field, uniform mesh refinement was preferred to the use of one-dimensional grid-clustering coordinate transformations.

1. INTRODUCTION

The past decade has witnessed a great deal of progress in the area of computational fluid dynamics. Developments in computer technology hardware as well as in advanced numerical algorithms have enabled attempts to be made towards analysis and numerical solution of highly complex flow problems. For some of these applications, the use of simple iterative techniques to solve the Navier–Stokes equations leads to a rather slow convergence rate for the solutions. The solution convergence rate can be seriously affected if the coupling among the various governing differential equations is not properly honored either in the interior of the solution domain or at its boundaries. The rate of convergence is also generally strongly dependent on such problem parameters as the Reynolds number, the mesh size, and the total number of computational points. This has led several researchers to examine carefully the recently emerging multigrid (MG) technique as a useful means for enhancing the convergence rate of iterative numerical methods for solving discretized equations at a number of computational grid points so large as to be considered impractical previously.

* This research was supported in part by AFOSR Grant 80-0160, with Dr. James D. Wilson as Technical Monitor.

0021-9991/82/120387-25$02.00/0

The theoretical potential of the multigrid method has been adequately exposed for the system of discretized equations arising from a single differential equation (e.g., [15, 22]). In fact, for 1–D problems, Merriam [15] has shown the likeness of the multigrid method to the direct solution procedure of cyclic reduction. This potential has been realized and demonstrated in actual solutions of sample problems [3, 5, 8, 13]. Application of the multigrid technique to the solution of a system of coupled nonlinear differential equations still poses several questions, however, that are currently being studied by various investigators [7, 21, 22].

The present study represents an effort to employ the multigrid method in the solution of the Navier–Stokes equations for a model flow problem with a goal of obtaining solutions for Reynolds numbers and mesh refinements as high as possible. The fundamental principle of the multigrid procedure is first described briefly, then its application to the governing equations is discussed in detail. Finally, the results obtained for the shear-driven flow in a square cavity at Reynolds number as high as 5000 and 10,000 are presented, together with the particular details that needed to be observed in obtaining these solutions.

2. Basic Principle of Multigrid Technique

Following Brandt and Dinar [7], the continuous differential problem considered is a system of l partial differential equations represented symbolically as

$$L_j \bar{U}(\bar{x}) = F_j(\bar{x}), \qquad j = 1, 2, \ldots, l, \quad \bar{x} \in D, \tag{2.1}$$

with the m boundary conditions

$$B_i \bar{U}(\bar{x}) = G_i(\bar{x}), \qquad i = 1, 2, \ldots, m, \quad \bar{x} \in \partial D, \tag{2.2}$$

where $\bar{U} = (U_1, U_2, \ldots, U_l)$ are the unknown variables, $\bar{x} = (x_1, x_2, \ldots, x_d)$ are the d independent variables of the d-dimensional problem, F_j and G_i are known functions on domain D and its boundary ∂D, respectively, and L_j and B_i are general differential operators.

A finite-difference solution to the problem described by Eqs. (2.1) and (2.2) is desired in a computational domain with grid spacing h. With a superscript h to denote the finite-difference approximation, the linear system of algebraic equations resulting from a selected difference scheme can be represented as

$$L_j^h \bar{U}^h(\bar{x}^h) = F_j^h(\bar{x}^h). \tag{2.3}$$

A conventional iterative technique for solving Eq. (2.3) consists of repeated sweeps of some relaxation scheme, the simplest being the Gauss–Seidel scheme, until convergence is achieved. It is often experienced that the convergence of the method is fast only for the first few iterations. This phenomenon can be explained if one considers a Fourier analysis of the error. Brandt [5] has thus estimated the

magnitude of the smoothing rate μ defined as the factor by which each error component is decreased during one relaxation sweep of the Gauss–Seidel procedure. It is observed that Gauss–Seidel relaxation produces a good smoothing rate for those error components whose wave length is comparable to the size of the mesh; the smoothing rate of more slowly varying Fourier components of the error is relatively poor. The multigrid method is based primarily on this feature. It recognizes that a wavelength which is long relative to a fine mesh is shorter relative to a coarser mesh. Hence, after the first two or three iterations on a given fine mesh, the multigrid method switches to a coarser mesh with step size $2h$, where the error components with wavelength comparable to $2h$ can be rapidly annihilated. The fine-grid solution determined in the first step then needs to be corrected to reflect appropriately the removal of the $2h$-wavelength content from the error. Repeated application of this process over a sequence of grids constitutes the basic idea of the multigrid method.

Accordingly, the multigrid method makes use of a hierarchy of computational grids D^k with the corresponding grid functions $\bar{U}^k$, $k = 1, 2, \ldots, M$. The step size on D^k is h_k and $h_{k+1} = \frac{1}{2}h_k$, so that as k decreases, D^k becomes coarser. On the kth grid, Eq. (2.1) has the discretized approximate form

$$L_j^k \bar{U}^k = F_j^k. \tag{2.4}$$

The operations of transfer of functions from fine to coarse grids or from coarse to fine grids, have been termed "interpolations" by Brandt [5]. This terminology is somewhat unconventional when referring to transfer from fine to coarse grids. The alternative terminology of restriction and prolongation, used by Hackbush [13] and Wesseling [22], for example, is preferred here. The restriction operator R_k^{k-1} transfers a fine-grid function $\bar{U}^k$ to a coarse-grid function $\bar{U}^{k-1}$. On the other hand, the prolongation operator, denoted as P_{k-1}^k, transfers a coarse-grid function $\bar{U}^{k-1}$ to a fine-grid function $\bar{U}^k$.

For the restriction operator, the simplest possible form is "injection," whereby the values of a function in the coarse grid are taken to be exactly the values at the corresponding points of the next fine grid, i.e.,

$$(R_k^{k-1} u^k)_{i+1,j+1} = u^k_{2i+1,2j+1}. \tag{2.5}$$

Being computationally efficient, injection has been used very frequently, particularly in the initial phases of development of a multigrid program. In general, however, the restriction operator R_k^{k-1} may be formulated as one of many possible weighted averages of neighboring fine-grid function values. Two such operators are the optimal-weighted averaging and the full-weighted averaging operators defined by Brandt [6]. It is significant to note that these two are equivalent for 1-D problems. For 2-D problems, optimal-weighted averaging involves fewer points than full-weighted averaging, which as the name indicates, involves all eight points $(i \pm \nu, j \pm \sigma)$, $\nu, \sigma = 0, 1$, adjacent to a given point (i, j). Hence, optimal weighting may be computationally more efficient than full weighting, but the latter provides better

stability and convergence properties to a multigrid technique, particularly for problems with rapidly varying coefficients. Full weighting is also preferred by Wesseling [22] who termed it "9-point restriction" because of the number of points it employs, i.e.,

$$\begin{aligned}(R_k^{k-1}u^k)_{i+1,j+1} = {} & \tfrac{1}{4}u^k_{2i+1,2j+1} \\ & + \tfrac{1}{8}[u^k_{2i+2,2j+1} + u^k_{2i+1,2j+2} + u^k_{2i,2j+1} + u^k_{2i+1,2j}] \\ & + \tfrac{1}{16}[u^k_{2i+2,2j+2} + u^k_{2i,2j+2} + u^k_{2i+2,2j} + u^k_{2i,2j}].\end{aligned} \tag{2.6}$$

Wesseling also tested a 7-point modification of the above 9-point restriction operator and found it to be almost equally suitable. The optimal-weighted averaging operator of Brandt [6] is a 5-point restriction operator derivable from Eq. (2.6) by eliminating the influence of the four corner-point values and doubling the center-point influence.

For the prolongation operator, the simplest form is derived using linear interpolation. This has been indicated by Brandt to be suitable for second-order differential equations. Prolongation by linear interpolation introduces no ambiguity when the interpolated value is desired at the midpoints of the boundaries of a mesh cell. Two options are possible, however, for obtaining the interpolated value at the center of a cell. The choice of R_k^{k-1} as defined by Eq. (2.6) suggests that the prolongation operator P_{k-1}^k also involve nine points so that the value at the cell center is obtained as the arithmetic mean of the four corner points. This leads to the 9-point prolongation operator defined by Wesseling as

$$\begin{aligned}(P_{k-1}^k u^{k-1})_{2i+1,2j+1} &= u^{k-1}_{i+1,j+1}, \\ (P_{k-1}^k u^{k-1})_{2i+2,2j+1} &= \tfrac{1}{2}[u^{k-1}_{i+1,j+1} + u^{k-1}_{i+2,j+1}], \\ (P_{k-1}^k u^{k-1})_{2i+1,2j+2} &= \tfrac{1}{2}[u^{k-1}_{i+1,j+1} + u^{k-1}_{i+1,j+2}], \\ (P_{k-1}^k u^{k-1})_{2i+2,2j+2} &= \tfrac{1}{4}[u^{k-1}_{i+1,j+1} + u^{k-1}_{i+2,j+1} + u^{k-1}_{i+1,j+2} + u^{k-1}_{i+2,j+2}].\end{aligned} \tag{2.7}$$

The operators defined in Eqs. (2.6) and (2.7) have the important property that P_{k-1}^k is the adjoint of R_k^{k-1}, i.e.,

$$\langle R_k^{k-1}u^k, v^{k-1}\rangle_{k-1} = \langle u^k, P_{k-1}^k v^{k-1}\rangle_k, \tag{2.8}$$

where $\langle\ \rangle$ denotes an inner product defined as

$$\langle u^k, v^k\rangle_k \equiv \frac{1}{h_k^2}\sum_{i,j} u^k_{i,j}v^k_{i,j}. \tag{2.9}$$

This properly maintains the coarse-grid equation to be a "homogenization" of the fine-grid equation [2]. This is particularly important for nonlinear problems. In finite-element discretization, this property leads to coarse-grid operators defined as

$$L^{k-1} = R_k^{k-1}L^kP_{k-1}^k = (P_{k-1}^k)^* L^kP_{k-1}^k. \tag{2.10}$$

Brandt and Dinar [7] indicate that the choice of the restriction operators is guided by rather definite rules, so that the only flexibility in a multigrid procedure is in the selection of the smoothing technique, i.e., the relaxation technique. While this may be true to an extent, even the limited experience of the present authors with the multigrid method indicates that, within the prescribed guidelines, some modifications in the restriction and the prolongation operators do influence the efficiency of the overall algorithm. Also, the definition of convergence in the finer grids appears to influence the final solution obtained.

3. Application to Navier–Stokes Equations for Shear-Driven Cavity Flow

The laminar incompressible flow in a square cavity whose top wall moves with a uniform velocity in its own plane has served over and over again as a model problem for testing and evaluating numerical techniques, in spite of the singularities at two of its corners. For moderately high values of the Reynolds number Re, published results are available for this flow problem from a number of sources (e.g., [9, 17, 19]), using a variety of solution procedures, including an attempt to extract analytically the corner singularities from the dependent variables of the problem [10]. Some results are also available for high Re [16], but the accuracy of most of these high-Re solutions has generally been viewed with some skepticism because of the size of the computational mesh employed and the difficulties experienced with convergence of conventional iterative numerical methods for these cases. Possible exceptions to these may be the results obtained by Benjamin and Denny [4] for $\mathrm{Re} = 10{,}000$ using a nonuniform 151×151 grid such that $\Delta x = \Delta y \simeq 1/400$ near the walls and those of Agarwal [1] for $\mathrm{Re} = 7500$ using a uniform 121×121 grid together with a higher-order accurate upwind scheme. The computational time required in these studies, however, is of the order of one hour or more for these high-Re solutions. The present study aims to achieve these solutions in a computational time that is considerably smaller, thereby rendering fine-mesh high-Re solutions more practical to obtain.

Governing Differential Equations and Boundary Conditions

With the nomenclature shown in Fig. 1, the two-dimensional flow in the cavity can be represented mathematically in terms of the stream function and the vorticity as follows, with the advective terms expressed in conservation form:

$$\text{Stream Function Equation:} \qquad \psi_{xx} + \psi_{yy} + \omega = 0. \tag{3.1}$$

Vorticity Transport Equation:

$$\omega_{xx} + \omega_{yy} - \mathrm{Re}[(\psi_y \omega)_x - (\psi_x \omega)_y] = \mathrm{Re}\, \omega_t. \tag{3.2}$$

Boundary conditions. The zero-slip condition at the nonporous walls yields that ψ and its normal derivatives vanish at all the boundaries. As is well known, this

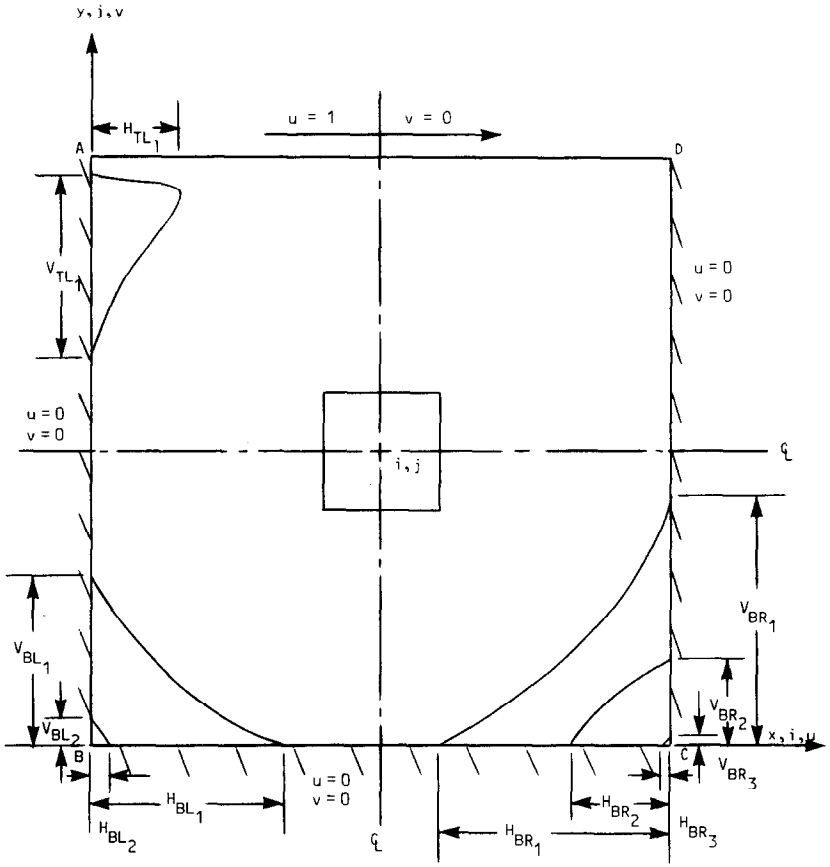

FIG. 1. Cavity flow configuration, coordinates, nomenclature, and boundary conditions.

provides no direct condition for ω at the walls. Theoretically, this should not pose a difficulty if the equations for ω and ψ are solved simultaneously and if all boundary conditions are imposed implicitly. In practice, however, the boundary conditions for ω are derived from the physical boundary conditions together with the definition of ω as given by Eq. (3.1).

Thus, at the moving wall $y = 1, j = J$:

$$\psi_J = 0, \tag{3.3}$$

$$\omega_J = -\psi_{yy} = -(\psi_{J+1} - 2\psi_J + \psi_{J-1})/\Delta y^2, \tag{3.4}$$

where ψ_{J+1} is evaluated from a third-order accurate finite-difference expression for ψ_{y_J} which is a known quantity at the boundary, i.e.,

$$\psi_{y_J} = (2\psi_{J+1} + 3\psi_J - 6\psi_{J-1} + \psi_{J-2})/(6\Delta y). \tag{3.5}$$

The resulting expression (3.4) for ω_j is then second-order accurate (see [12]).

Expressions for ω at other boundaries are obtained in an analogous manner.

Discretization

The discretization is performed on a uniform mesh. In fact, with a multigrid solution technique, nonuniform mesh or grid-clustering coordinate transformations are not essential since local mesh refinement may be achieved by defining progressively finer grids in designated subdomains of the computational region. Second-order accurate central finite-diferrence approximations are employed for all second-order derivatives in Eqs. (3.1) and (3.2). The convective terms in Eq. (3.2) are represented via a first-order accurate upwind difference scheme including its second-order accurate term as a deferred correction, as formally suggested by Khosla and Rubin [14]. This ensures diagonal dominance for the resulting algebraic equations, thus lending the necessary stability property to the evolving solutions while restoring second-order accuracy at convergence.

Relaxation Scheme (Smoothing Operator)

In the multigrid method, the role of the iterative relaxation scheme is not so much to reduce the error as to smooth it, i.e., to eliminate the high-frequency error components. Due to the coupling between governing equations (3.1) and (3.2) as well as through the vorticity boundary conditions (Eq. (3.4)), sequential relaxation of the individual equations (3.1) and (3.2) would have poor smoothing rate. For example, smooth errors in ψ could produce high-frequency error components in the vorticity solution via the boundary condition for ω. On the other hand, a convergent solution of each equation at each step would constitute a very inefficient procedure. An appropriate approach consists of relaxing the coupled governing equations (3.1) and (3.2) simultaneously and incorporating the vorticity boundary conditions implicitly. A coupled Gauss–Seidel procedure or a coupled alternating–directing implicit scheme may be used for this purpose. Rapid convergence, however, of the coarsest-grid solution as required in the full multigrid algorithm [6] can be safely assured by the use of these methods only when the coarsest mesh is not too fine. On the other hand, for the driven-cavity flow at high Re, too coarse a grid does not retain enough of the solution features and cannot, therefore, provide an appropriate initial approximation to the fine-grid solution for high-Re flow. Hence, the present work employs the coupled strongly implicit (CSI) procedure of Rubin and Khosla [18]. This scheme is a two-equation extension of the strongly implicit procedure developed by Stone [20] for a scalar elliptic equation and may be viewed as a generalization of the Thomas algorithm to two-dimensional implicit solutions. Its effectiveness has been demonstrated by Rubin and Khosla [18] via application to a number of flow problems. The present authors have also found it to be useful in conjunction with the multigrid technique [11]. The procedure may be approximately likened to incomplete lower–upper (ILU) decomposition which is considerably more efficient, manifesting lower values of the smoothing factor μ than the simple Gauss–Seidel relaxation procedure.

Prolongation and Restriction Operators

The prolongation operator was always chosen to be the 9-point operator given in Eq. (2.7) except for converged coarse-grid solutions where cubic interpolations were used as suggested by Brandt [6]. For the restriction operator, simple injection as well as the 5-point operator (optimal weighting) and the 9-point operator (Eq. (2.6)) were employed. While the first two generally provided convergent solutions, 9-point restriction led to improved convergence for the very high Re cases computed.

Multigrid Procedure

For the present nonlinear problem, the full approximation scheme (FAS) was employed, rather than a correction scheme. Also, the full multigrid (FMG) algorithm was preferred over the cycling algorithm since a converged coarse-grid solution is generally obtainable by the CSI procedure used for relaxation. It is possible that, for the higher-Re cases computed, the cycling algorithm could also be used with the first approximation of the finest-grid solution being provided by the solution of a preceding calculation with a lower value of Re. Finally, the "accommodative" version of the multigrid procedure was used so that convergence as well as convergence rate were monitored during the process of relaxation on a given grid in order to control the computational procedure, particularly with respect to switching from one grid to another. The accommodative FAS–FMG procedure used here follows that detailed by Brandt [6]. This procedure is briefly described below.

The solution on grid D^k is denoted as u^k. This is prolongated to the next finer grid D^{k+1} using the prolongation operator to provide an estimate for u^{k+1} as

$$u_{\text{est}}^{k+1} = P_k^{k+1} u^k. \tag{3.6}$$

This estimate is used as the initial guess for the solution on grid D^{k+1}, i.e., for solving the equation

$$L^{k+1} u^{k+1} = F^{k+1}. \tag{3.7}$$

Convergence is defined to occur when the norm e_{k+1} of the dynamic residuals of Eq. (3.7) is below a specified tolerance, ε_{k+1}, i.e.,

$$e_{k+1} < \varepsilon_{k+1}, \tag{3.8}$$

with ε_{k+1} taken to be 10^{-4} in the present work. It must be recognized that this assigned value for ε_{k+1} remains in effect only until the first multigrid cycle is executed, during which ε_{k+1} is redefined as described later in Eqs. (3.13) and (3.14). During the relaxation process, the convergence rate for Eq. (3.7) is also monitored and compared with the theoretical smoothing rate of the relaxation procedure used. Accordingly, if the ratio of the residuals e_{k+1}^n and e_{k+1}^{n+1} for two consecutive iterations n and $(n+1)$ is smaller than the smoothing rate of the scheme, the iteration process is continued. Following convergence, k is incremented by unity and the steps indicated by Eqs. (3.6) and (3.7) are repeated. This is continued until $k = M$, i.e., convergence on the desired finest grid is achieved, yielding the required final solution.

If, at any stage of the relaxation process for $k \neq 1$, i.e., for all but the coarsest grid, the convergence rate is not satisfactory, i.e., if

$$e_{k+1}^{n+1}/e_{k+1}^{n} > \eta, \tag{3.9}$$

where $\eta = \mu$, the scheme smoothing rate, then a multigrid cycle is interjected in the procedure. The multigrid cycle consists of computing a coarse-grid correction u_{k+1}^{k} to the evolving fine-grid solution u_{old}^{k+1} by solving the equation

$$L^k u_{k+1}^{k} = f^k, \tag{3.10}$$

where

$$f^k \triangleq L^k(R_{k+1}^{k} u_{\text{old}}^{k+1}) + R_{k+1}^{k}(f^{k+1} - L^{k+1} u_{\text{old}}^{k+1}). \tag{3.11}$$

If $(k+1)$ is currently the finest level, then $f^{k+1} \equiv F^{k+1}$. This correction is used to improve the old fine-grid solution according to the relation

$$u_{\text{new}}^{k+1} = u_{\text{old}}^{k+1} + P_k^{k+1}(u_{k+1}^{k} - R_{k+1}^{k} u_{\text{old}}^{k+1}). \tag{3.12}$$

Convergence of Eq. (3.10) is defined to occur when the residual norm e_k for this equation is smaller than the residual norm e_{k+1} for the finer grid, i.e., when

$$e_k < \varepsilon_k = \delta e_{k+1} \tag{3.13}$$

where $\delta < 1$; the value used was $\delta = 0.2$.

Following the correction according to Eq. (3.12), the solution of Eq. (3.7) proceeds as before.

If the solution of Eq. (3.10) itself does not exhibit a satisfactory convergence rate, defined in a manner analogous to Eq. (3.9), then a second multigrid cycle may be performed by going to a yet coarser grid D^{k-1} to enhance the convergence rate of Eq. (3.10). Thus, a sequence of multigrid cycles may be nested, one inside another, to solve the current finest-grid equation efficiently. On the currently finest grid D^{k+1} in this nest, convergence should be attained to within the estimated truncation error τ_k so that, corresponding to Eq. (3.8) the convergence criterion used is

$$e_{k+1} < \varepsilon_{k+1} = \alpha^q \tau_k, \tag{3.14}$$

where τ_k is the norm of $(F^k - f^k)$, $\alpha = (h_{k+1}/h_k)^2$, and $q = 1$ for second-order accurate discretization. As will be discussed in the next section, modification of Eq. (3.14) to include α^q, with $q > 1$, appears to influence the converged numerical values of the solution.

4. Fine-Grid and High-Re Results for Driven Cavity

The correctness of the analysis, the solution procedure, and the computer program were assessed by first obtaining fine-mesh solutions for the case with $\text{Re} = 100$ for which ample reliable results are available in the literature. This case was also intended for experimentation with some of the parameters associated with the

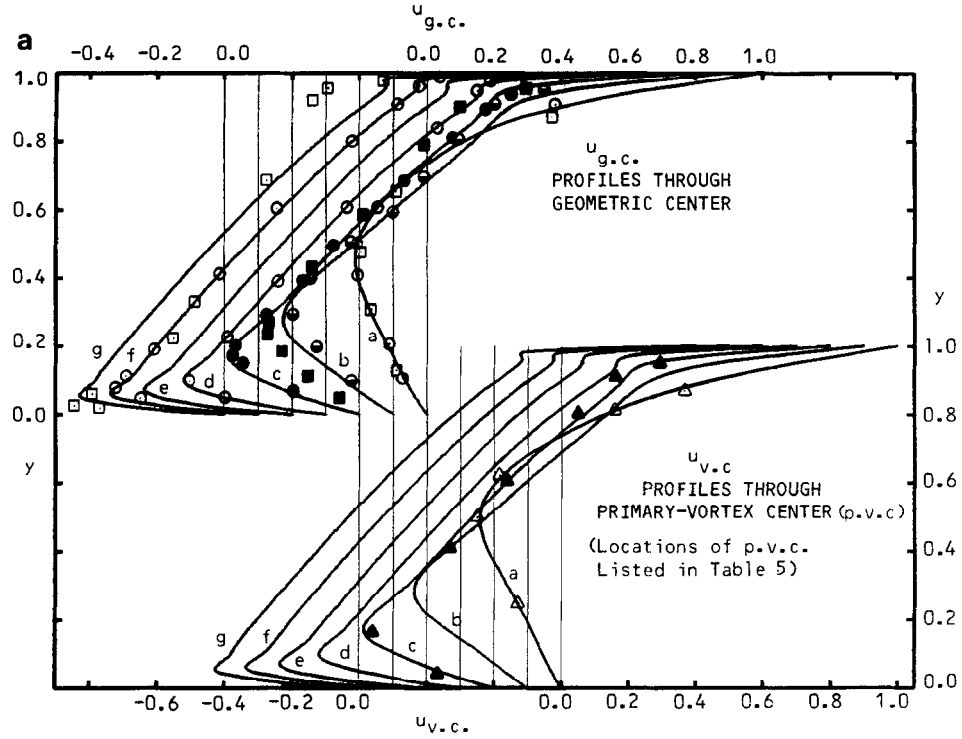

FIG. 2a. Comparison of u-velocity along vertical lines through geometric center and primary vortex center.

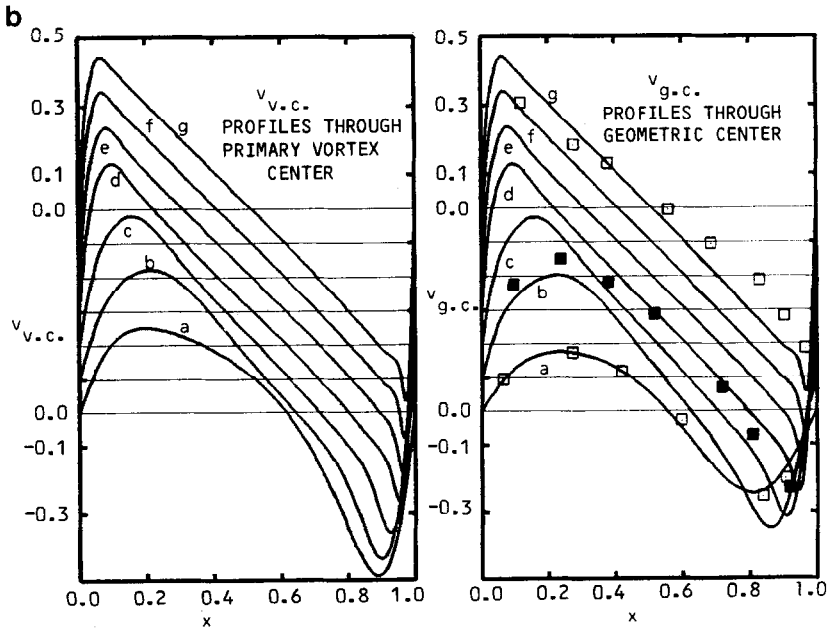

FIG. 2b. Comparison of profiles of v-velocity along horizontal lines through geometric center and primary vortex center.

multigrid procedure, namely, selection of η in Eq. (3.9), values q_ψ and q_ω for q in Eq. (3.14), the coarsest mesh width, the finest mesh width h_M, and the prolongation and restriction operators. It was observed that h_M is the most important parameter, especially for high Re. Also, as Re increased, very coarse grids could not be included in the procedure. The smoothing factor μ for the CSI procedure used is expected to be smaller than that for the Gauss–Seidel scheme. Nevertheless, for $\mathrm{Re} = 100$ and 400, $\eta = 0.5$ was used. The value of η had to be increased gradually with Re; for $\mathrm{Re} = 10{,}000$, $\eta = 0.7$ was needed. Similarly, a time step of infinity could be used in the vorticity equation for Re up to 3200 but had to be reduced rather rapidly as Re increased. For $\mathrm{Re} = 10{,}000$, $\Delta t = 0.1$ was required. The corresponding values Δt_ω used by Benjamin and Denny [4] in conjunction with the ADI solution procedure for the case with $\mathrm{Re} = 10{,}000$ were smaller than this by several orders of magnitude; this may also partly explain the reduction in computational time achieved by the present solution technique. Initially, $q = 1$ was used in Eq. (3.14). For $\mathrm{Re} = 100$, this proved adequate in the respect that the results agreed well with available solutions. But for $\mathrm{Re} \geqslant 1000$, the values obtained, for instance, for $|\psi_{\min}|$ at the center of the primary vortex were somewhat lower than the published solutions. Better comparison resulted from the use of $q > 1$. This is because increasing q enforces continuation of the iteration process and leads to some further reduction of the dynamic residuals e_{k+1}, while also modifying the actual solution simultaneously. The results published by most previous investigators have been obtained subject to the convergence criterion that the relative change in two successive iterates of the solution at each computational point be below a prescribed small value. Frequently, the choice of this value is not related to the truncation error in the finite-difference approximation. On the other hand, in the present computational procedure, convergence on the finest grid is defined in terms of the truncation error. Hence, the results presented here employed $q_\omega = 4$ and $q_\psi = 5$, except for the cases with $\mathrm{Re} = 7500$ and 10,000 which used $q_\psi = 4$.

Figures 2a and b show the velocity profiles for u along vertical lines and v along

LEGEND

Re / Source	100	400	1000	3200	5000	7500	10000
	a	b	c	d	e	f	g
Present	—	—	—	—	—	—	—
Rubin and Khosla [1977]	△		▲				
Nallasamy & Prasad [1977]	□		■				□
Agarwal [1981]	○	◒	●	○		○	

horizontal lines passing through the geometric center of the cavity and through the center of the primary vortex in the flow. The origins for these graphs for various values of Re have been displaced for clarity of the profiles. The thinning of the wall boundary layers with increase in Re is evident from these profiles, although the rate of this thinning is very slow for $Re \geqslant 5000$. The near-linearity of these velocity profiles in the central core of the cavity is indicative of the uniform vorticity region that develops here for large Re. The high-Re profiles of u exhibit a kink near $y = 1$, while a similar behavior is observed for the v profiles near $x = 1$. Such behavior has been reported by some previous investigators, and is seen to persist in the present fine-grid solutions. This would imply that the velocity distributions near these walls are not extremely sensitive to mesh size. The values of ψ and ω at the vortex center are observed to be considerably more sensitive to mesh size than these velocity profiles.

Included in Fig. 2 are the available results of [1, 16, 17]. For $Re = 100$, all results agree well with one another as well as with the present solutions, indicating that for this value of Re, the coarser grids employed by the previous investigators were quite adequate. As Re increases, however, the inadequacy of coarse meshes gradually becomes apparent. This is particularly evident in the solutions reported by Nallasamy

TABLE I

Results for u-velocity along Vertical Line through Geometric Center of Cavity

129-grid pt. no.	y	Re						
		100	400	1000	3200	5000	7500	10,000
129	1.00000	1.00000	1.00000	1.00000	1.00000	1.00000	1.00000	1.00000
126	0.9766	0.84123	0.75837	0.65928	0.53236	0.48223	0.47244	0.47221
125	0.9688	0.78871	0.68439	0.57492	0.48296	0.46120	0.47048	0.47783
124	0.9609	0.73722	0.61756	0.51117	0.46547	0.45992	0.47323	0.48070
123	0.9531	0.68717	0.55892	0.46604	0.46101	0.46036	0.47167	0.47804
110	0.8516	0.23151	0.29093	0.33304	0.34682	0.33556	0.34228	0.34635
95	0.7344	0.00332	0.16256	0.18719	0.19791	0.20087	0.20591	0.20673
80	0.6172	−0.13641	0.02135	0.05702	0.07156	0.08183	0.08342	0.08344
65	0.5000	−0.20581	−0.11477	−0.06080	−0.04272	−0.03039	−0.03800	0.03111
59	0.4531	−0.21090	−0.17119	−0.10648	−0.86636	−0.07404	−0.07503	−0.07540
37	0.2813	−0.15662	−0.32726	−0.27805	−0.24427	−0.22855	−0.23176	−0.23186
23	0.1719	−0.10150	−0.24299	−0.38289	−0.34323	−0.33050	−0.32393	−0.32709
14	0.1016	−0.06434	−0.14612	−0.29730	−0.41933	−0.40435	−0.38324	−0.38000
10	0.0703	−0.04775	−0.10338	−0.22220	−0.37827	−0.43643	−0.43025	−0.41657
9	0.0625	−0.04192	−0.09266	−0.20196	−0.35344	−0.42901	−0.43590	−0.42537
8	0.0547	−0.03717	−0.08186	−0.18109	−0.32407	−0.41165	−0.43154	−0.42735
1	0.0000	0.00000	0.00000	0.00000	0.00000	0.00000	0.00000	0.00000

and Prasad [16]. Nevertheless, the fourth-order accurate spline method of Rubin and Khosla [17] remains satisfactory with a 17×17 mesh at $Re = 1000$. Also, the third-order accurate scheme of Agarwal [1] performs well with a 121×121 grid at $Re = 7500$, but the corresponding computer time is quite large. Unfortunately, Benjamin and Denny [4] did not present any velocity data, although their solutions are considered to be very accurate for high Re.

In view of the above remarks, the present fine-mesh results should be very useful. Consequently, Tables I and II list the numerical values corresponding to the velocity profiles shown in Fig. 2 for lines passing through the geometric center of the cavity. Only typical points, rather than the entire large set of computational points, along these profiles have been listed. Care has been taken to include the points of local maxima and minima for all values of Re; these points are underscored.

The streamline contours for the cavity flow configurations with Re increasing from 100 to 10,000 are shown in Fig. 3. A magnified view of the various secondary vortices is also included. The values of ψ along the contours shown are listed in Table III. For $Re = 400$, the results from a 129×129 grid as well as a 257×257 grid are presented in order to demonstrate that the 129×129 grid is adequate for moderate values of Re. Although a comparison is not shown in this figure, the extent

TABLE II

Results for v-Velocity along Horizontal Line through Geometric Center of Cavity

129-grid pt. no.	x	Re						
		100	400	1000	3200	5000	7500	10,000
129	1.0000	0.00000	0.00000	0.00000	0.00000	0.00000	0.00000	0.00000
125	0.9688	–0.05906	–0.12146	–0.21388	–0.39017	–0.49774	–0.53858	–0.54302
124	0.9609	–0.07391	–0.15663	–0.27669	–0.47425	–0.55069	–0.55216	–0.52987
123	0.9531	–0.08864	–0.19254	–0.33714	–0.52357	–0.55408	–0.52347	–0.49099
122	0.9453	–0.10313	–0.22847	–0.39188	–0.54053	–0.52876	–0.48590	–0.45863
117	0.9063	–0.16914	–0.23827	–0.51550	–0.44307	–0.41442	–0.41050	–0.41496
111	0.8594	–0.22445	–0.44993	–0.42665	–0.37401	–0.36214	–0.36213	–0.36737
104	0.8047	–0.24533	–0.38598	–0.31966	–0.31184	–0.30018	–0.30448	–0.30719
65	0.5000	0.05454	0.05186	0.02526	0.00999	0.00945	0.00824	0.00831
31	0.2344	0.17527	0.30174	0.32235	0.28188	0.27280	0.27348	0.27224
30	0.2266	0.17507	0.30203	0.33075	0.29030	0.28066	0.28117	0.28003
21	0.1563	0.16077	0.28124	0.37095	0.37119	0.35368	0.35060	0.35070
13	0.0938	0.12317	0.22965	0.32627	0.42768	0.42951	0.41824	0.41487
11	0.0781	0.10890	0.20920	0.30353	0.41906	0.43648	0.43564	0.43124
10	0.0703	0.10091	0.19713	0.29012	0.40917	0.43329	0.44030	0.43733
9	0.0625	0.09233	0.18360	0.27485	0.39560	0.42447	0.43979	0.43983
1	0.0000	0.00000	0.00000	0.00000	0.00000	0.00000	0.00000	0.00000

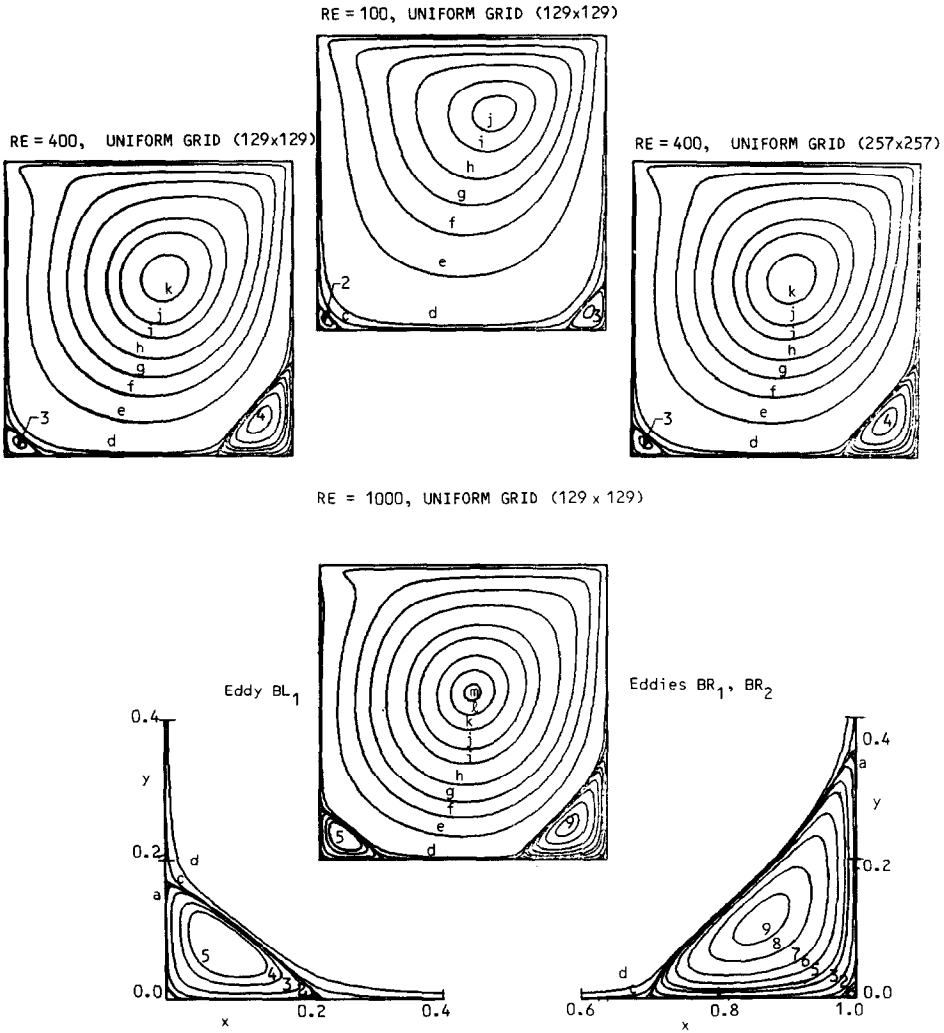

FIG. 3. Streamline pattern for primary, secondary, and additional corner vortices.

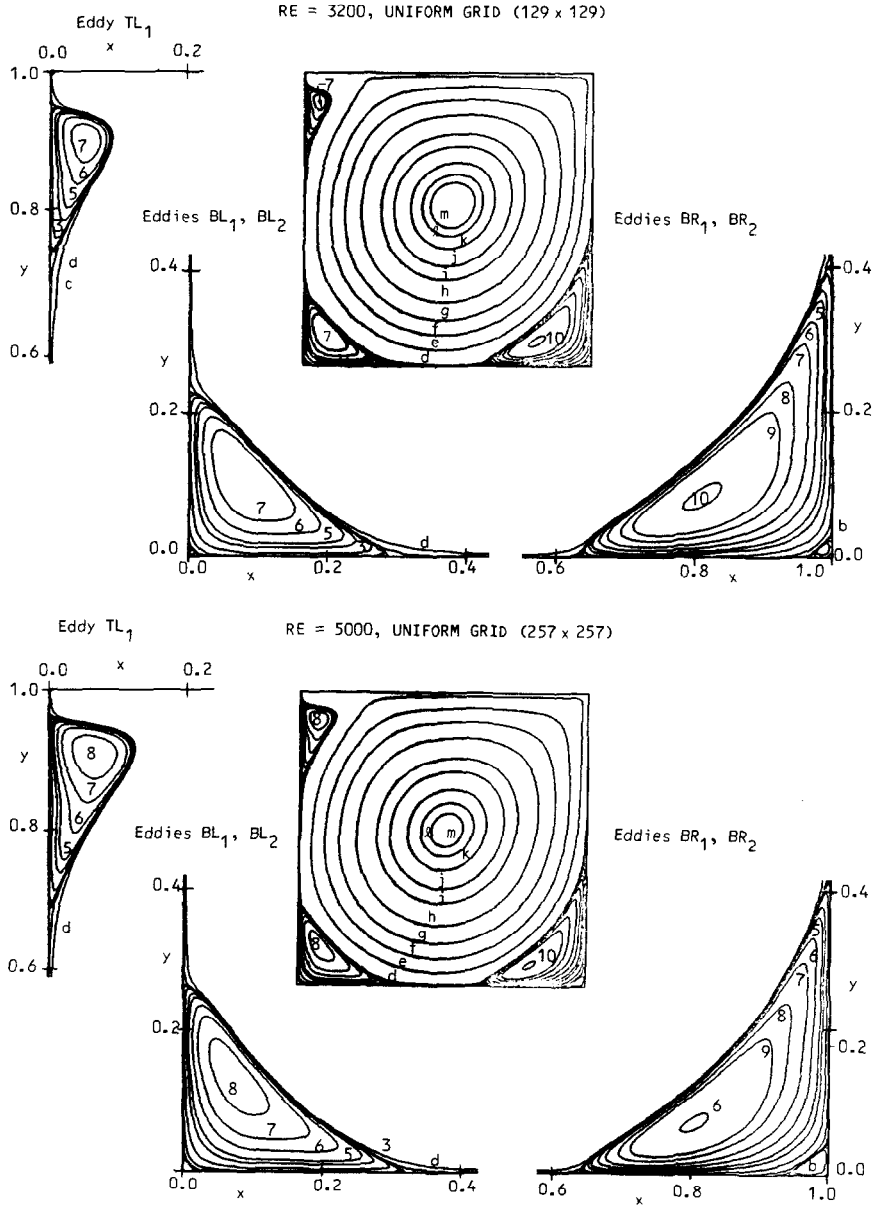

FIGURE 3 *(continued)*

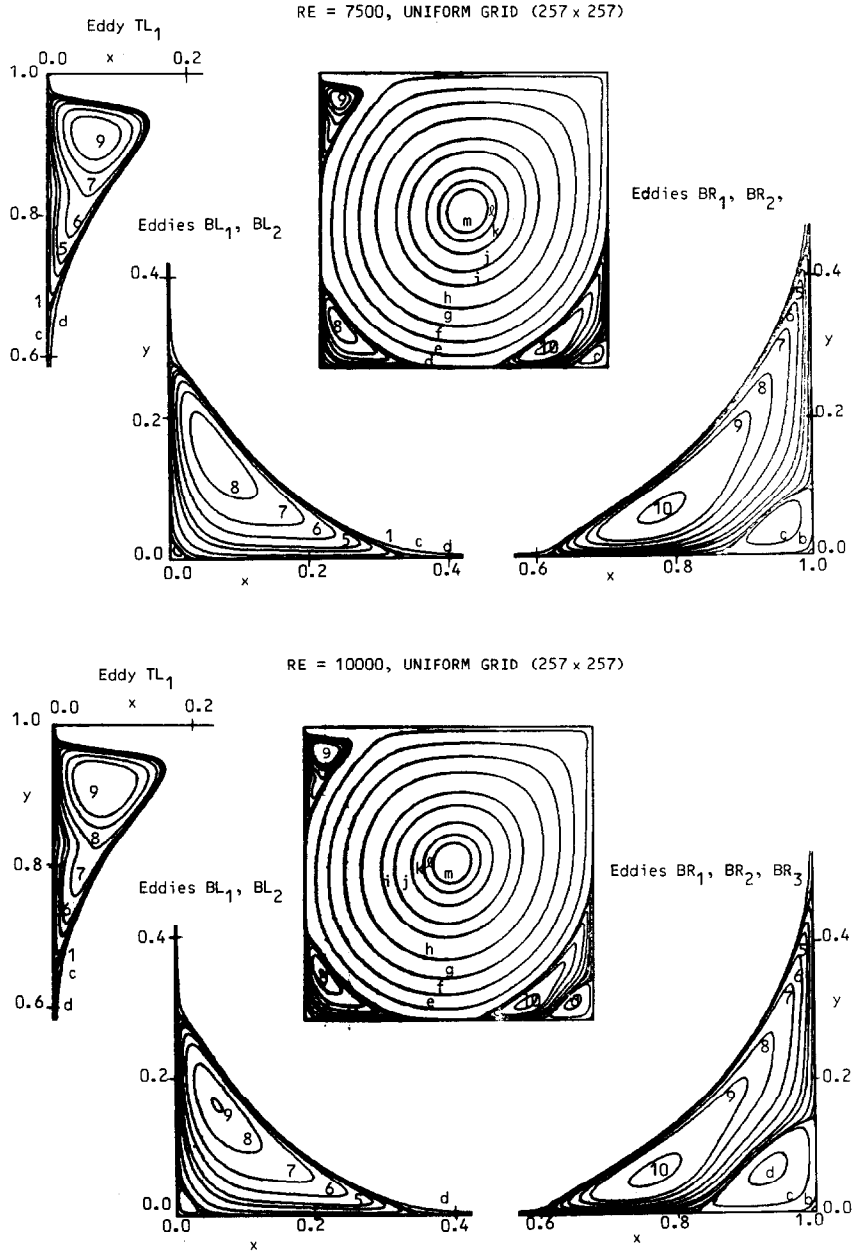

FIGURE 3 *(concluded)*

TABLE III

Values for Streamline and Vorticity Contours in Figs. 3 and 4

Stream function				Vorticity	
Contour letter	Value of ψ	Contour number	Value of ψ	Contour number	Value of ω
a	-1.0×10^{-10}	0	1.0×10^{-8}	0	0.0
b	-1.0×10^{-7}	1	1.0×10^{-7}	±1	±0.5
c	-1.0×10^{-5}	2	1.0×10^{-6}	±2	±1.0
d	-1.0×10^{-4}	3	1.0×10^{-5}	±3	±2.0
e	−0.0100	4	5.0×10^{-5}	±4	±3.0
f	−0.0300	5	1.0×10^{-4}	5	4.0
g	−0.0500	6	2.5×10^{-4}	6	5.0
h	−0.0700	7	5.0×10^{-4}		
i	−0.0900	8	1.0×10^{-3}		
j	−0.1000	9	1.5×10^{-3}		
k	−0.1100	10	3.0×10^{-3}		
l	−0.1150				
m	−0.1175				

of the various secondary vortices is in excellent agreement with that reported by Benjamin and Denny [4]. The present results, however, are computationally more efficient.

In Fig. 4 we show the vorticity contours corresponding to the streamline patterns presented in Fig. 3. Again, the values of ω along these contours are listed in Table III. As Re increases, several regions of high vorticity gradients, indicated by concentration of the vorticity contours, appear within the cavity. It is seen from Fig. 4 that these regions are not aligned with the geometric boundaries of the cavity. It is for these reasons that uniform mesh refinement was used in the present study. Possible suitable alternatives appear to be the use of a basically modified non-Cartesian coordinate system and of a solution-adaptive local mesh refinement. An often-compared quantity for cavity flows is the vorticity at the midpoint of the moving wall or the minimum value of ω at this boundary. Hence, the values of ω at several selected points along this boundary are listed in Table IV, with the minimum value indicated by the underscore. These values of $\omega_{\min}$ agree very well with the results tabulated in [4].

As seen from Figs. 3 and 4, fine-mesh solutions exhibit additional counter-rotating vortices in or near the cavity corners as Re increases. The effect of Re on the location of the centers of these vortices is shown in Fig. 5. In terms of the notation shown in Fig. 1, the letters T, B, L, and R denote top, bottom, left, and right, respectively; the subscript numeral denotes the hierarchy of these secondary vortices. Thus, BR_2 refers to the second in the sequence of secondary vortices that occur in the bottom right corner of the cavity. As is well known, the center of the primary vortex is offset

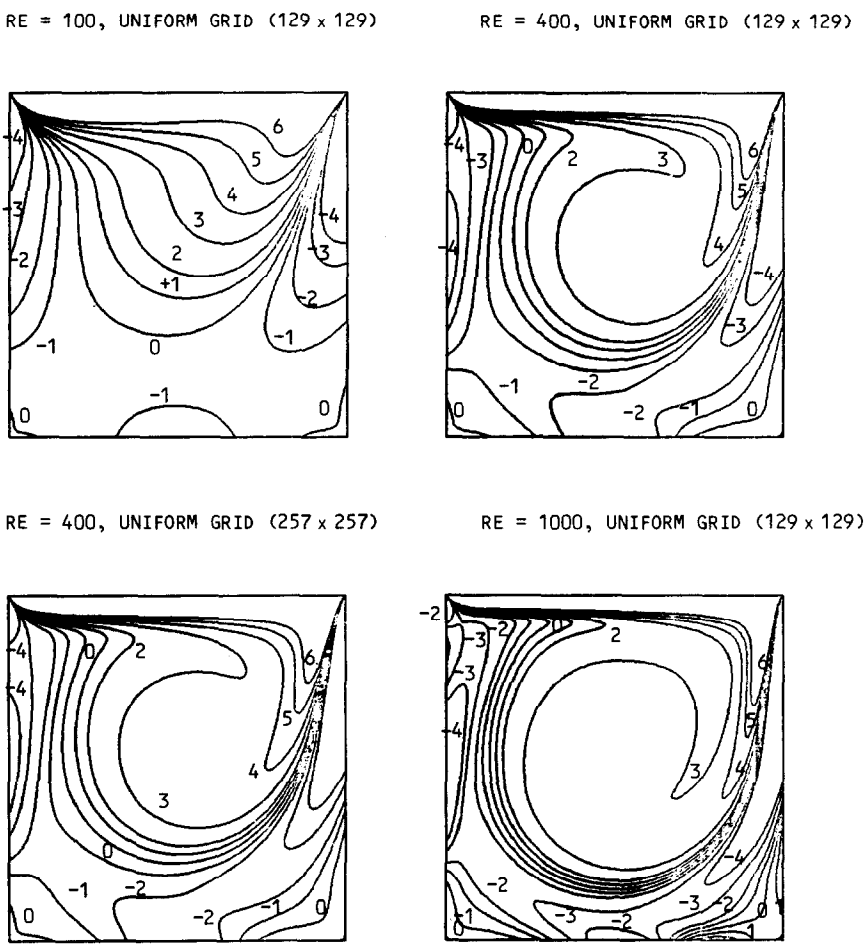

FIG. 4. Vorticity contours for flow in driven cavity.

towards the top right corner at Re = 100. It moves towards the geometric center of the cavity with increase in Re. Its location becomes virtually invariant for Re $\geqslant$ 5000. All the secondary vortices appear initially very near the corners (or near the wall, in the case of the vortex TL_1) and their centers also move, though very slowly, towards the cavity center with increase in Re. At the larger values of Re considered, the convection of these secondary eddies is evidenced by the direction of movement of the centers of these vortices.

The computational advantage gained by use of the MG procedure is best illustrated in terms of the behavior of the root-mean square (RMS) value of the dynamic residuals of the discretized governing equations in the finest grid. In Fig. 6 we show the finest-grid RMS residuals for ψ and ω obtained during a single-grid computation with $h = \frac{1}{128}$ (solid curve) as well as a multigrid calculation with $h_M = \frac{1}{128}$ and $M = 6$

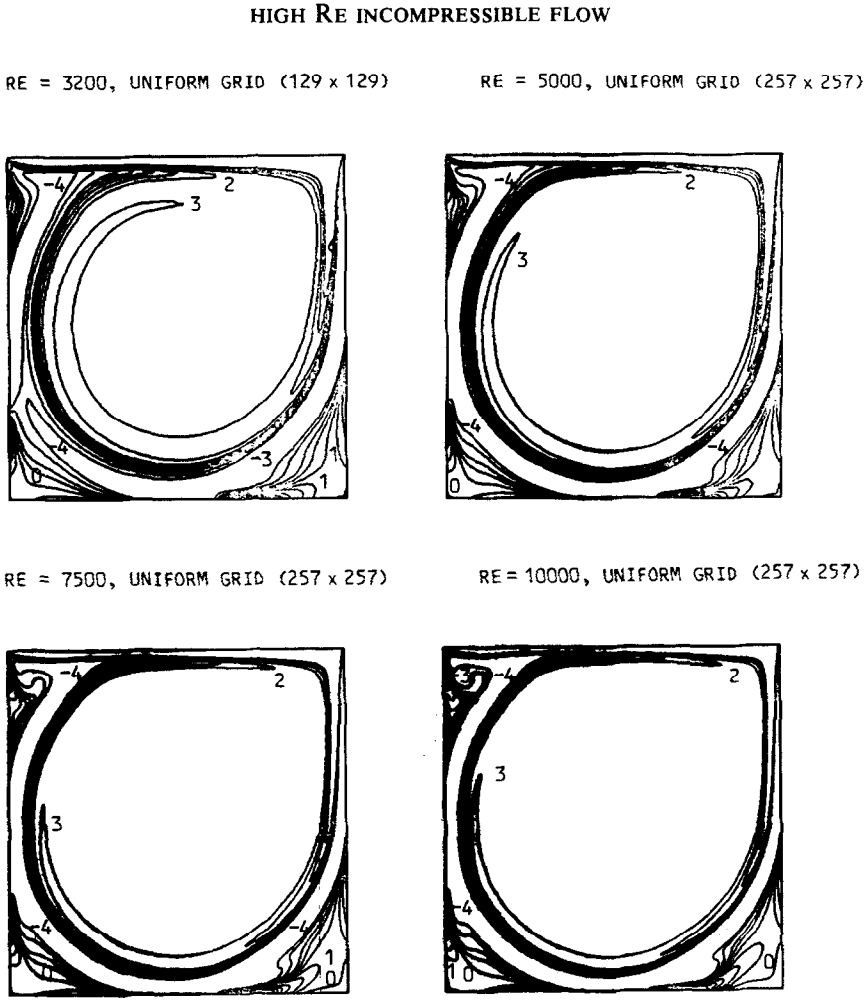

FIGURE 4 *(continued)*

(solid and dashed lines). Flow configurations with Re = 100 and Re = 1000 have been examined. In both cases, even the single-grid calculations exhibit a rapid initial decay of the RMS residuals for ψ as well as ω during the first 4–6 iterations (work units). Thereafter, the solid curves show a marked decrease in their slope. Employing the multigrid process after these first 4–6 work units tends to retain the initial decay rate for the errors during the overall computation.

It is important to mention two points with respect to the MG curves in Fig. 6. First, the solid portions of the MG-curves correspond to the relaxation step (smoothing) on the finest grid while the dashed portions correspond to the coarse-grid correction due to the MG cycle. Second, although convergence was defined on the basis of the arithmetic average of the RMS residual in ω and ψ, the convergence rate was examined in terms of the RMS residual in ω alone. It is perhaps for this reason

TABLE IV

Results for Vorticity ω along Moving Boundary

	Re						
x	100	400	1000	3200	5000	7500	10,000
0.0000	-	-	-	-	-	-	-
0.0625	40.0110	53.6863	75.5980	126.670	146.702	180.927	209.452
0.1250	22.5378	34.6351	51.0557	89.3391	103.436	125.131	145.073
0.1875	16.2862	26.5825	40.5437	75.6401	91.5682	111.115	127.928
0.2500	12.7844	21.0985	32.2953	61.7864	77.9509	98.2364	116.275
0.3125	10.4199	16.8900	25.4341	47.1443	60.0065	75.6334	90.0231
0.3750	8.69628	13.7040	20.2666	35.8795	45.8622	56.9345	67.1400
0.4375	7.43218	11.4537	16.8350	28.9413	37.3609	45.9128	53.5905
0.5000	6.57451	10.0545	14.8901	25.3889	33.0115	40.3982	46.8271
0.5625	6.13973	9.38889	14.0928	24.1457	31.3793	38.3834	44.3287
0.6250	6.18946	9.34599	14.1374	24.4639	31.5791	38.6951	44.6303
0.6875	6.82674	9.88979	14.8061	25.8572	33.0486	40.6123	46.8672
0.7500	8.22110	11.2018	16.0458	27.9514	35.3504	43.5641	50.3792
0.8125	10.7414	13.9068	18.3120	30.4779	38.0436	46.8901	54.3725
0.8750	15.6591	19.6859	23.8707	34.2327	41.3394	50.0769	57.7756
0.9375	30.7923	35.0773	42.1124	49.9664	56.7091	61.4046	66.0352
1.0000	—	—	—	—	—	—	—

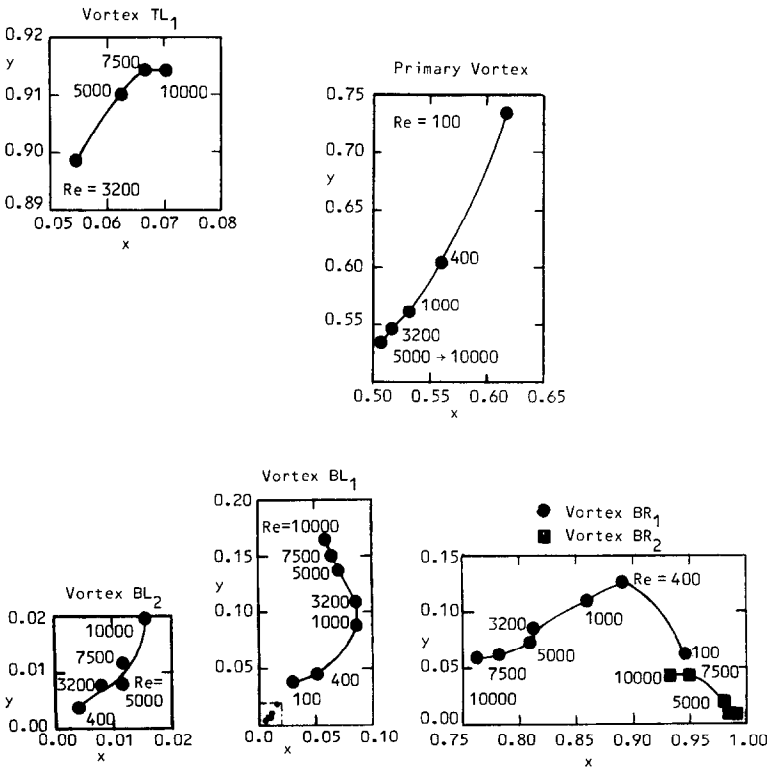

FIG. 5. Effect of Reynolds number on location of vortex centers.

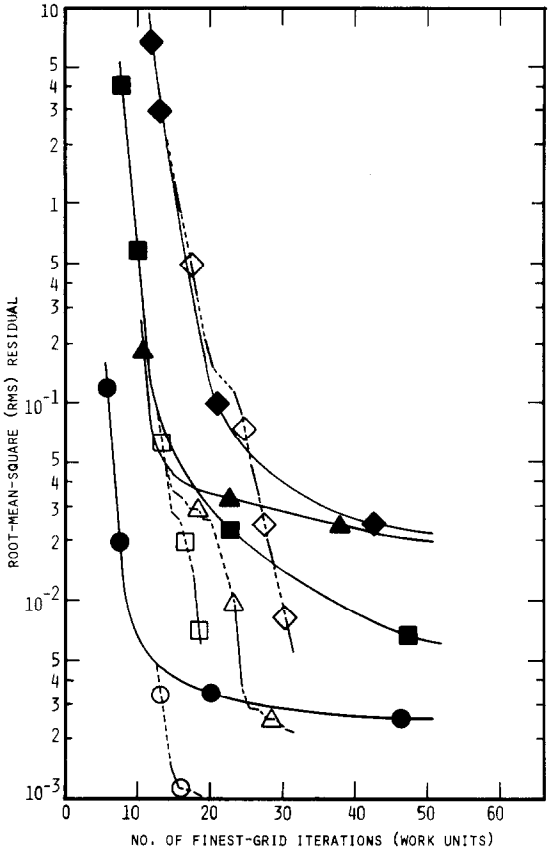

FIG. 6. Convergence of single grid and multigrid computational procedures. Single grid ($h = \frac{1}{128}$) Re = 100: (●) e_ψ, (■) e_ω; Re = 1000: (▲) e_ψ, (◆) e_ω. Multigrid ($h_M = \frac{1}{128}$, $M = 6$) Re = 100: (○) e_ψ, (□) e_ω; Re = 1000: (△) e_ψ, (◇) e_ω.

that ω exhibits a much more desirable convergence behavior than ψ because the convergence rate is indeed the parameter that comprises the basis for interjecting an MG cycle in the solution procedure. Some further improvement in the overall convergence process may be possible by also including the convergence rate of ψ in the criterion controlling switching to the coarse-grid correction step.

Finally, a comprehensive survey of the properties of the primary and secondary vortices in the driven-cavity flow is provided in Table V. Some of these are directly comparable with the numerical data listed in [1, 4]. In particular, attention is drawn to the values of $\psi_{\min}$ and $\omega_{v.c.}$ for the primary vortex. The present calculations for Re = 7500 with a 257×257 grid exhibit a stronger secondary vortex BR_2 than reported by Agarwal [1]. Consequently, the present primary vortex is somewhat weakened. Nevertheless, the approach of $\omega_{v.c.}$ to the infinite-Re value of 1.886 is clear, although this value is approached "from below" for the present solutions.

TABLE

Properties of Primary

Number	Property	100	400	1000
Primary	ψ_{min}	−0.103423	−0.113909	−0.117929
	$\omega_{v.c.}$	3.16646	2.29469	2.04968
	Location, x, y	0.6172, 0.7344	0.5547, 0.6055	0.5313, 0.5625
First	ψ_{max}	—	—	—
T	$\omega_{v.c.}$	—	—	—
	Location, x, y	—	—	—
	H_L	—	—	—
	V_L	—	—	—
BL	ψ_{max}	1.74877×10^{-6}	1.41951×10^{-5}	2.31129×10^{-4}
	$\omega_{v.c.}$	-1.55509×10^{-2}	-5.69697×10^{-2}	−0.36175
	Location, x, y	0.0313, 0.0391	0.0508, 0.0469	0.0859, 0.0781
	H_L	0.0781	0.1273	0.2188
	V_L	0.0781	0.1081	0.1680
BR	ψ_{max}	1.25374×10^{-5}	6.42352×10^{-4}	1.75102×10^{-3}
	$\omega_{v.c.}$	-3.30749×10^{-2}	-4.33519×10^{-1}	−1.15465
	Location, x, y	0.9453, 0.0625	0.8906, 0.1250	0.8594, 0.1094
	H_L	0.1328	0.2617	0.3034
	V_L	0.1484	0.3203	0.3536
Second	ψ_{min}	—	-7.67738×10^{-10}	—
BL	$\omega_{v.x.}$	—	9.18377×10^{-4}	—
	Location, x, y	—	0.0039, 0.0039	—
	H_L	—	0.0039	—
	V_L	—	0.0039	—
BR	ψ_{min}	—	-1.86595×10^{-8}	-9.31929×10^{-8}
	$\omega_{v.c.}$	—	4.38726×10^{-3}	8.52782×10^{-3}
	Location, x, y	—	0.9922, 0.0078	0.9922, 0.0078
	H_L	—	0.0156	0.0078
	V_L	—	0.0156	0.0078
Third	ψ_{max}	—	—	—
BR	Location, x, y	—	—	—
	H_L	—	—	—
	V_L	—	—	—
Work units		18.84	18.08	31.56
CPU seconds		53.59	215.05	92.27
Mesh points		129	257	129

V

and Secondary Vortices

Re			
3200	5000	7500	10,000
−0.120377	−0.118966	−0.119976	−0.119731
1.98860	1.86016	1.87987	1.88082
0.5165, 0.5469	0.5117, 0.5352	0.5117, 0.5322	0.5117, 0.5333
7.27682×10^{-4}	1.45641×10^{-3}	2.04620×10^{-3}	2.42103×10^{-3}
−1.71161	−2.08843	−2.15507	−2.18276
0.0547, 0.8984	0.0625, 0.9102	0.0664, 0.9141	0.0703, 0.9141
0.0859	0.1211	0.1445	0.1589
0.2057	0.2693	0.2993	0.3203
9.7823×10^{-4}	1.36119×10^{-3}	1.46709×10^{-3}	1.51829×10^{-3}
−1.06301	−1.53055	−1.78511	−2.08560
0.0859, 0.1094	0.0703, 0.1367	0.0645, 0.1504	0.0586, 0.1641
0.2844	0.3184	0.3339	0.3438
0.2305	0.2643	0.2793	0.2891
3.13955×10^{-3}	3.08358×10^{-3}	3.28484×10^{-3}	3.41831×10^{-3}
−2.27365	−2.66354	−3.49312	−4.0531
0.8125, 0.0859	0.8086, 0.0742	0.7813, 0.0625	0.7656, 0.0586
0.3406	0.3565	0.3779	0.3906
0.4102	0.4180	0.4375	0.4492
-6.33001×10^{-8}	-7.08860×10^{-8}	-1.83167×10^{-7}	-7.75652×10^{-7}
1.44550×10^{-2}	1.88395×10^{-2}	1.72980×10^{-2}	2.75450×10^{-2}
0.0078, 0.0078	0.0117, 0.0078	0.0117, 0.0117	0.0156, 0.0195
0.0078	0.0156	0.0234	0.0352
0.0078	0.0163	0.0254	0.0441
-2.51648×10^{-7}	-1.43226×10^{-6}	-3.28148×10^{-5}	-1.31321×10^{-4}
9.74230×10^{-3}	3.19311×10^{-2}	1.41058×10^{-1}	3.12583×10^{-1}
0.9844, 0.0078	0.9805, 0.0195	0.9492, 0.0430	0.9336, 0.0625
0.0254	0.0528	0.1270	0.1706
0.0234	0.0417	0.0938	0.1367
—	—	1.58111×10^{-9}	5.66830×10^{-9}
—	—	0.9961, 0.0039	0.9961, 0.0039
—	—	0.0039	0.0039
—	—	0.0039	0.0039
78.25	70.8125	68.50	99.5
207.26	734.49	705.62	986.65
129	257	257	257

SUMMARY

Fine-mesh solutions have been obtained very efficiently for high-Re flow using the coupled strongly implicit and multigrid methods. The various operators and parameters in the multigrid procedure were examined, especially for high-Re flow. The use of 9-point restriction, or full-weighting, was found to be superior to 5-point restriction, or optimal weighting. The finest mesh size employed in the grid sequence continues to be a very significant parameter. The smoothing factor of the iteration scheme was seen to be influenced by the physical problem parameters, namely, Re. The definition used for convergence on current fine grids was also observed to influence the final solutions.

The robustness and the efficiency of the overall solution technique has been demonstrated using the model problem of flow in a driven square cavity. Detailed accurate results have been presented for this problem. Up to 257×257, i.e., 66049 computational points and Re as high as 10,000 have been considered, with CPU time of 16 to 20 minutes on the AMDAHL 470 V/6 computer. The present results agree well with published fine-grid solutions but are about four times as efficient.

Future effort includes consideration of primitive-variable formulation; true 3-D solutions may be possible in the foreseeable future, with practical CPU time requirements, by use of multigrid techniques.

REFERENCES

1. R. K. AGARWAL, "A Third-Order-Accurate Upwind Scheme for Navier–Stokes Solutions at High Reynolds Numbers," AIAA Paper No. 81-0112, 1981.
2. I. BABUSKA, *in* "Numerical Solutions of Partial Differential Equations III" (B. Hubbard, Ed.), Academic Press, New York, 1975.
3. N. S. BAKHVALOV, *USSR Comput. Math. Phys.* **6**(5) (1966), 101.
4. A. S. BENJAMIN AND V. E. DENNY, *J. Comput. Phys.* **33** (1979), 340.
5. A. BRANDT, *Math. Comput.* **31** (1977), 333.
6. A. BRANDT, "Multi-Level Adaptive Computations in Fluid Dynamics," AIAA Paper No. 79-1455, 1979.
7. A. BRANDT AND N. DINAR, *in* "Numerical Methods for Partial Differential Equations" (S. Parter, Ed.), Academic Press, New York, 1979.
8. R. P. FEDORENKO, *USSR Comput. Math. Phys.* **1** (1962), 1092.
9. K. N. GHIA, W. L. HANKEY, AND J. K. HODGE, "Study of Incompressible Navier–Stokes Equations in Primitive Variables Using Implicit Numerical Technique," AIAA Paper No. 77-648, 1977; *AIAA J.* **17**(3) (1979), 298.
10. K. N. GHIA, C. T. SHIN, AND U. GHIA, "Use of Spline Approximations for Higher-Order Accurate Solutions of Navier–Stokes Equations in Primitive Variables," AIAA Paper No. 79-1467, 1979.
11. K. N. GHIA, U. GHIA, C. T. SHIN, AND D. R. REDDY, *in* "Computers in Flow Predictions and Fluid Dynamics Experiments" (K. Ghia *et al.*, Eds.) ASME Publication, New York, 1981.
12. U. GHIA, K. N. GHIA, S. G. RUBIN AND P. K. KHOSLA, *Comput. Fluids* **9** (1981), 123.
13. W. HACKBUSCH, *Computing* **20** (1978), 291.
14. P. K. KHOSLA AND S. G. RUBIN, *Comput. Fluids* **2** (1974), 207.
15. M. L. MERRIAM, "Formal Analysis of Multi-Grid Techniques Applied to Poisson's Equations in Three Dimensions," AIAA Paper No. 81-1028, 1981.

16. M. NALLASAMY AND K. K. PRASAD, *J. Fluid Mech.* **79**(2) (1977), 391.
17. S. G. RUBIN AND P. K. KHOSLA, *J. Comput. Phys.* **24**(3) (1977), 217.
18. S. G. RUBIN AND P. K. KHOSLA, *Comput. Fluids* **9** (1981), 163.
19. R. E. SMITH AND A. KIDD, "Comparative Study of Two Numerical Techniques for the Solution of Viscous Flow in a Driven Cavity," pp. 61–82, NASA SP-378, 1975.
20. H. L. STONE, *SIAM J. Numer. Anal.* **5**(3) (1968), 530.
21. T. THUNELL AND L. FUCHS, *in* "Proceedings of Symposium on Numerical Methods in Laminar and Turbulent Flow" (C. Taylor, K. Morgan, and B. A. Schrefler, Eds.), pp. 141–152, Venice, Italy, 1981.
22. P. WESSELING, "Theoretical and Practical Aspects of a Multi-Grid Method," Report NA-37, Delft University of Technology, The Netherlands, 1980.